Directing the pore size of rigid polyurethane foam via controlled air entrainment

Martin Hamann, Sébastien Andrieux, Markus Schütte, Daniel Telkemeyer, Meik Ranft, Wiebke Drenckhan

Directing the pore size of rigid polyurethane foam via controlled air entrainment

Martin Hamann[1], Sébastien Andrieux[1], Markus Schütte[2], Daniel Telkemeyer[2], Meik Ranft[3]
Wiebke Drenckhan[1]

[1]CNRS-UPR 22, Institut Charles Sadron, Université de Strasbourg, 67200 Strasbourg, France
[2]BASF Polyurethanes GmbH, 49448 Lemförde, Germany
[3]BASF SE, 67056 Ludwigshafen am Rhein, Germany

Abstract

The interest in polyurethane rigid ("PUR") foams as potent thermally insulating materials for a wide range of applications continues to grow as the minimization of CO_2 emissions has become a global issue. Controlling the thermal insulation efficiency of PUR foams starts with the control of their morphology. Although the presence of micrometric air bubbles originating from air entrainment during the blending of the PU reactive mixture has been shown to influence the final PUR foam morphology, detailed experimental investigations on how exactly they affect the final PUR foam pore size are still lacking. To fill this gap, we use a double-syringe mixing device, which allows to control the number of air bubbles generated during a first air entrainment step, before using the same device to blend the reactive components in a sealed environment avoiding further air entrainment. Keeping all experimental parameters except for the air bubble density in the reactive mixture constant, we can correlate changes of the final PUR foam morphology with the variation of the air bubble density in the initially liquid reactive mixture. Our results confirm recent findings which suggest the presence of two different regimes of bubble nucleation and growth depending on the presence or absence of dispersed air bubbles in the liquid reactive mixture. Our study pushes those insights further by demonstrating an inverse relation between the air bubble density in the liquid reactive mixture and the final pore volume of the PUR foam. For example, at constant chemical formulation and blending conditions, we could vary the final pore size between 400-1600 µm simply by controlling the amount of pre-dispersed air bubbles within the system. We are confident that the presented approach may not only provide a valuable model experiment to scan formulations in R&D laboratories, but it may also provide suggestions for the optimization of industrial processes.

Keywords: PUR foam, air bubbles, nucleation, pore size, morphology, double-syringe mixing

Introduction

In the wake of increasing environmental awareness, reducing carbon dioxide emission has become a major declared goal of politics and society. Among others, heating and refrigeration significantly contribute to the global annual carbon dioxide output.[1,2] In this context, efficient thermal insulation of buildings, refrigerators, storage tanks etc. has become an important topic for both academic research and industry. As a consequence, interest in the optimization of polyurethane rigid (PUR) foams for thermal insulation applications has been revived in the last years,[3–11] since they excel with very low thermal conductivities.[12,13] Key to successful optimization of the physical properties of PUR foams for thermal insulation is their porous morphology[14–16]. For thermally insulating rigid foams in particular, a desirable foam morphology is characterized by small, closed pores with a narrow pore size distribution.[15–18] To develop strategies allowing for efficient control over the porous foam morphology, it is crucial to understand the main mechanisms involved in PUR foam formation. In general, formulations for the preparation of PUR foams consist of two components. The so-called "A-component" consists mainly of polyols but typically also contains additives such as surfactants, catalysts, and blowing agents.[19,20] The "B-component" usually only consists of (poly-)isocyanates. Shortly after both components are mixed, a crosslinked PU network via the polyaddition[21] of polyols and (poly-)isocyanates starts to form. In parallel, foam blowing takes place as inert low boiling point blowing agents evaporate due to the strongly exothermic nature of the polyaddition reaction. Besides physical blowing agent evaporation, additional blowing is achieved chemically by adding water which reacts with isocyanates to liberate CO_2.[19] Once the urethane network formation has sufficiently progressed, the initially liquid matrix becomes solid, hence "freezing" the cellular structure of the blown liquid foam.

Before the onset of PU network formation and foam blowing, micrometric air bubbles are entrapped into the system due to the (pre-)processing procedure, e.g. during the homogenization of the A-component and particularly during the vigorous mixing of the A- and B-component, which results in a bubbly, reactive mixture that eventually forms the PUR foam. The importance of these pre-dispersed air bubbles in fixing the final foam morphology was predicted decades ago.[22,23] It was suggested by Kanner et al.[22] that these dispersed air bubbles may serve as "precursors" for the pores of the final PUR foam, since the released blowing agent vapors may diffuse into them without any energy barrier to overcome (type IV non-classical nucleation[24]) and that there are typically sufficient air bubbles to account for all the pores found in the final PUR foam.[22] Peculiarly, this topic has received little experimental coverage for a long time and

related studies were published only in the past few years.[4,6,7] For instance, Merillas et al.[7] demonstrated very recently that the addition of solid nanoclay particles as nucleating agents hardly affects PUR foam morphology if they are dispersed within the system under vacuum. The authors argued that the vacuum prevents the particles from incorporating tiny air bubbles into the liquid reactive mixture while being dispersed and that only the air bubbles affect PUR foam morphology, not the nanoclay particles themselves. This is in line with findings by Brondi et al.[6] who showed that there are two types of bubble nucleation regimes in nascent PUR foam systems depending on whether dispersed air bubbles are present in the reactive mixture or not. Without dispersed bubbles, classical homogeneous bubble nucleation caused by gas supersaturation of the liquid phase is observed, while in the presence of dispersed bubbles, the existing bubbles take up all the released vapor of the blowing agent and the CO_2 without the nucleation of new bubbles.

If pore formation in PUR foams is in fact mostly driven by the inflation of entrapped air bubbles, the air bubble density within the initially liquid reactive mixture should dictate the pore size of the final PUR foam. To prove this hypothesis, we developed a new double-syringe processing technique which not only allows for controlling the number of micrometric air bubbles that are entrapped into the reactive mixture (Figure 1a and SI Figure S1), but also prevents further air entrainment during the blending step of the A- and B-component. Additionally, the loss of volatile blowing agents during processing is inhibited, since the setup is sealed. The double-syringe mixing technique as such has already been reported in the literature for the generation of liquid- and solid foams[25,26] as well as emulsions[27–29]. However, to the best of our knowledge, this study is the first report on the exploitation of this technique in connection with PUR foam systems. Employing this processing and mixing technique together with a simplified model PUR foam formulation, we show that dispersed micrometric air bubbles indeed affect PUR foam morphology crucially and, most importantly, that there is a direct relation between the initial air bubble density in the reactive mixture forming the PUR foam and the mean pore size of the final PUR foam.

Experimental approach, results and discussion

Air entrainment

The first step of our process is the controlled generation of bubbles via air entrainment into the A-component only. For all experiments conducted in this study, the A-component consists of tripropylene glycol (TPG; 93.95 wt%), an amine-based reaction catalyst (1.55 wt% of the A-component), a polysiloxane-based surfactant (2.00 wt% of the A-component), water (2.50 wt% of the A-component) as chemical blowing agent, and cyclopentane as physical blowing agent (13.5 wt% with respect to 100% A-component added *on top*). Detailed information on the PUR foam formulation and preparation is provided in the supporting information (SI, Section 1). As sketched in Figure 1a, 17 ml of the A-component are poured into a 60 ml plastic syringe and attached to another 60 ml plastic syringe filled with 17 ml of air via a narrow silicone tubing (internal diameter d_{int} = 3.2 mm ; external diameter d_{ext} = 4.8 mm) and a three-way valve. Then, the connected syringes are fixed within a home-built double-syringe mixing device[26] which drives a periodical motion of a two-armed crankshaft to push the pistons of the connected syringes in an alternating fashion. Thus, the content of both syringes is pushed repeatedly through the narrow tubing which leads to the formation of air bubbles via air entrainment into the polyol-based A-component. A more detailed description of the setup is provided in the supporting information (SI, Section 2). This polyol-based A-component containing air bubbles is what we refer to as "premix" in the following. The double-syringe technique allows for an explicit control of the premix generation for several reasons:

1. The ratio between liquid and gas in the syringes can be set precisely.
2. The velocity of the crankshaft movement, i.e. the energy input, can be varied.
3. The number of mixing cycles, i.e. the mixing time, can be varied.
4. The system is sealed. Thus, uncontrolled air entrainment from the environment into the system is prevented as well as loss of volatile blowing agents due to evaporation.

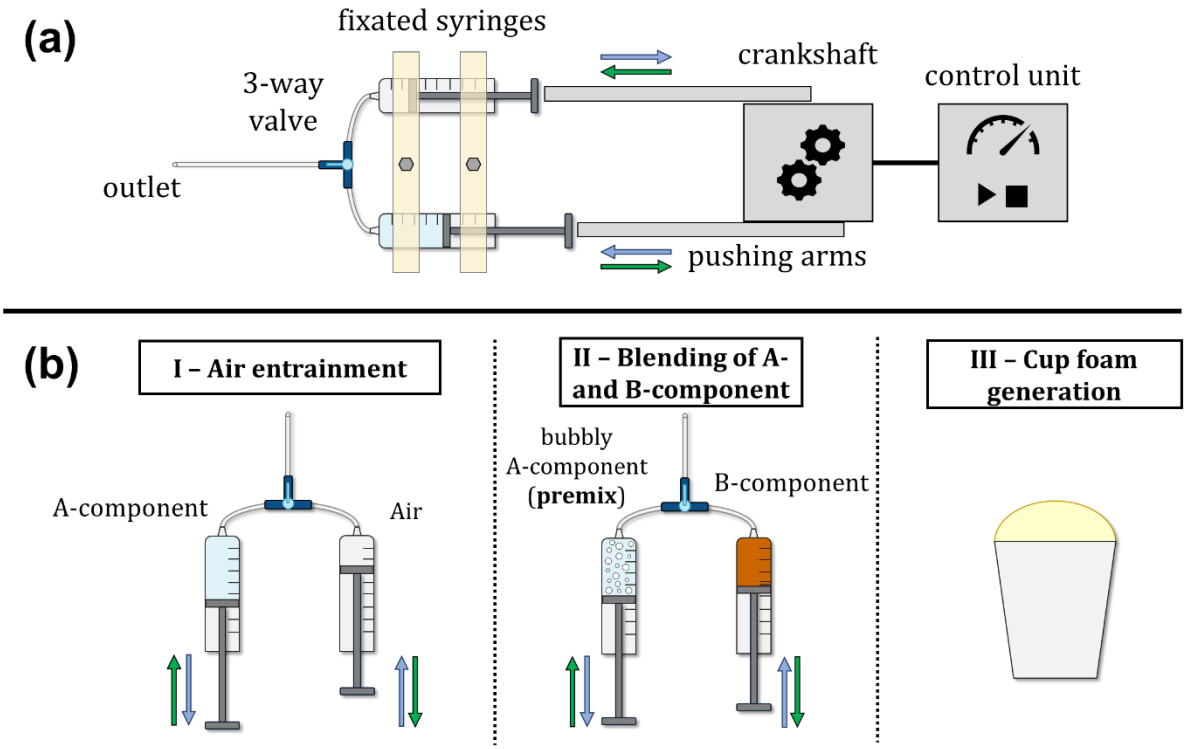

Figure 1: (a) Schematic drawing of the double-syringe device used for bubble generation via air entrainment and blending of reactive PUR foam formulations. (b) Three-step process used to generate the premix and the liquid reactive mixture with a controlled number of micrometric air bubbles before foam blowing.

To alter the number of air bubbles formed during the air entrainment step (see step I in Figure 1b), we varied the number of mixing cycles N_c between air and the A-component while keeping the average speed of the crankshaft arms constant at $\langle v \rangle$ = 9 cm s^{-1}. To be more precise, we chose six different conditions of the air entrainment step with N_c being [0 ; 1 ; 2 ; 5 ; 10 ; 50]. For each N_c, a sample of the premix is collected directly after the air entrainment step and analyzed using transmitted light microscopy. Automatic image analysis via *ImageJ* is used to measure the number of entrained air bubbles per unit volume of the premix, i.e. the bubble density ω_{pre}, and the mean bubble radius $\langle R_b \rangle$. For detailed information on the microscopy analysis, the reader is referred to the supporting information (SI, Section 3.1). An overview over the observed bubble densities ω_{pre} and the mean bubble radii $\langle R_b \rangle$ obtained in the premix directly after the air entrainment step for different numbers of air entrainment cycles N_c is provided in Figure 2. Note that for each cycle number N_c, the air entrainment experiments were repeated and analyzed at least three times.

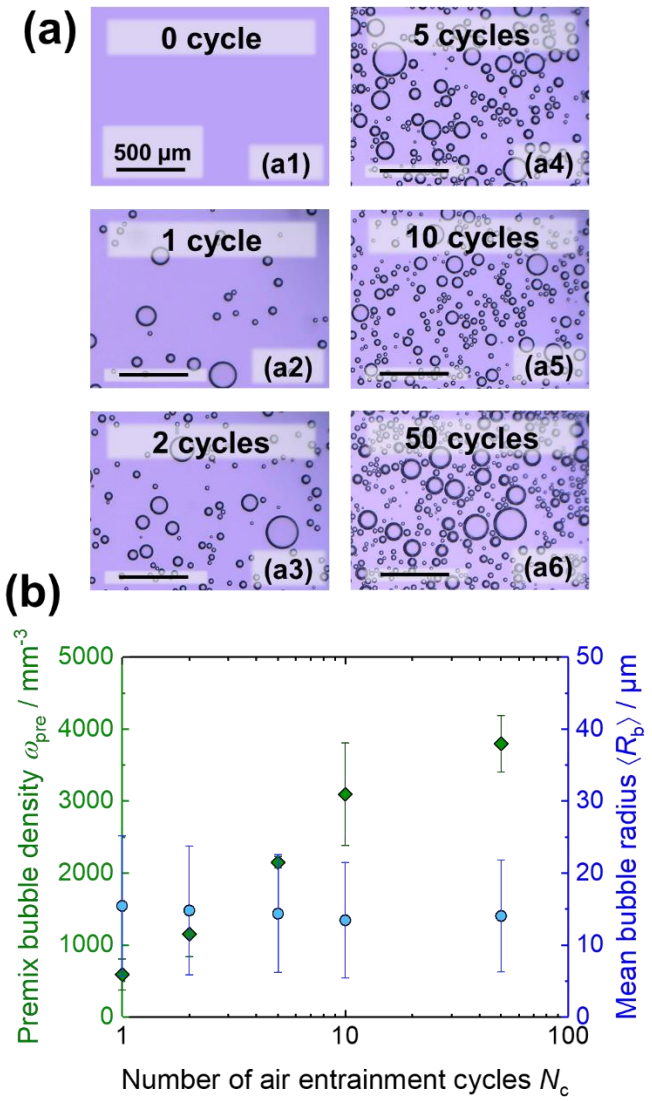

Figure 2: (a) Transmitted light microscopy photographs of bubbly, polyol-based A-components (premix) directly after the air entrainment step for different numbers of air entrainment cycles N_c. (b) Measured air bubble density in the premix ω_{pre} after air entrainment (green diamonds) and the corresponding mean bubble radii $\langle R_b \rangle$ (blue circles) for different numbers of air entrainment cycles N_c in the double-syringe device.

The microscopy images (Figure 2a) as well as the diagram in Figure 2b reveal that increasing the number of air entrainment cycles N_c leads to a steady increase of the air bubble density ω_{pre} in the premix. Premixes with air bubble densities ω_{pre} ranging between 0 and roughly 4000 bubbles per mm^3 can hence be obtained in a highly reproducible manner. In contrast, the mean bubble radius $\langle R_b \rangle$ is hardly affected by the number of air entrainment cycles N_c since $\langle R_b \rangle$ remains constant between 13 – 15 µm. These findings confirm that the chosen double-syringe process is very well-suited for studying the relationship between the air bubble density ω_{pre} in the premix (and therefore also in the reactive mixture) prior to PUR foam formation and the

final PUR foam morphology, as it provides good control over the bubble formation during air entrainment.

PUR foam preparation

Directly after the air entrainment step, the whole premix is collected in only one of the two syringes (step II in Figure 1b), while the opposite empty syringe is replaced as quickly as possible (typically 40-50 seconds) by a syringe filled with the B-component (oligomeric methylene diphenyl diisocyanate, 198 wt% with respect to A-component; NCO-Index = 120). Blending of the reactive components, i.e. the now bubbly A-component (premix) and the B-component, is then conducted using three cycles of pushing back and forth both components through the connecting constriction with the double-syringe device. Note that three blending cycles proved to be appropriate to obtain sufficiently homogeneously dispersed "reactive mixtures" of the A-and B-component (see supporting information, Section 3.2), while being short enough to prevent premature foam blowing, i.e. foam blowing inside the syringes during the blending step. As the system is sealed, additional air entrainment and evaporation of volatile components during the blending step of the reactive components is avoided. This is another major advantage of the double-syringe technique, since for most other blending approaches uncontrolled evaporation takes place and air is trapped into the matrix arbitrarily *while* the reactive compounds are being blended.[23] The double-syringe process therefore allows to trace back potential changes in PUR foam morphology exclusively to variations of the initial air bubble density ω in the liquid reactive mixture, given that all other process parameters are kept constant (e.g. PUR foam formulation, blending step conditions). After blending, the liquid reactive mixture is ejected via the outlet channel of the three-way valve into a paper cup (V = 735 ml) where foam blowing and solidification take place. Finally, 3-5 days after complete foam solidification, photographs of the whole foam and of cubes cut out of the center of the foam are taken. Moreover, the porous morphology is analyzed via scanning electron microscopy (SEM) (see SI, Section 4). Photographs and SEM images of the PUR foams that were obtained using reactive mixtures of different air bubble density ω are provided in Figure 3. Note that "ω" refers to the air bubble density in the reactive mixture, while "ω_{pre}" refers to the bubble density of the premix. To obtain ω from ω_{pre}, we consider the volumetric dilution of the bubble density in the premix upon addition of the B-component during the blending step, i.e.

$$\omega = \frac{V_{\mathrm{A}}}{V_{\mathrm{A}}+V_{\mathrm{B}}}\,\omega_{\mathrm{pre}} = 0.38\,\omega_{\mathrm{pre}}. \qquad [1]$$

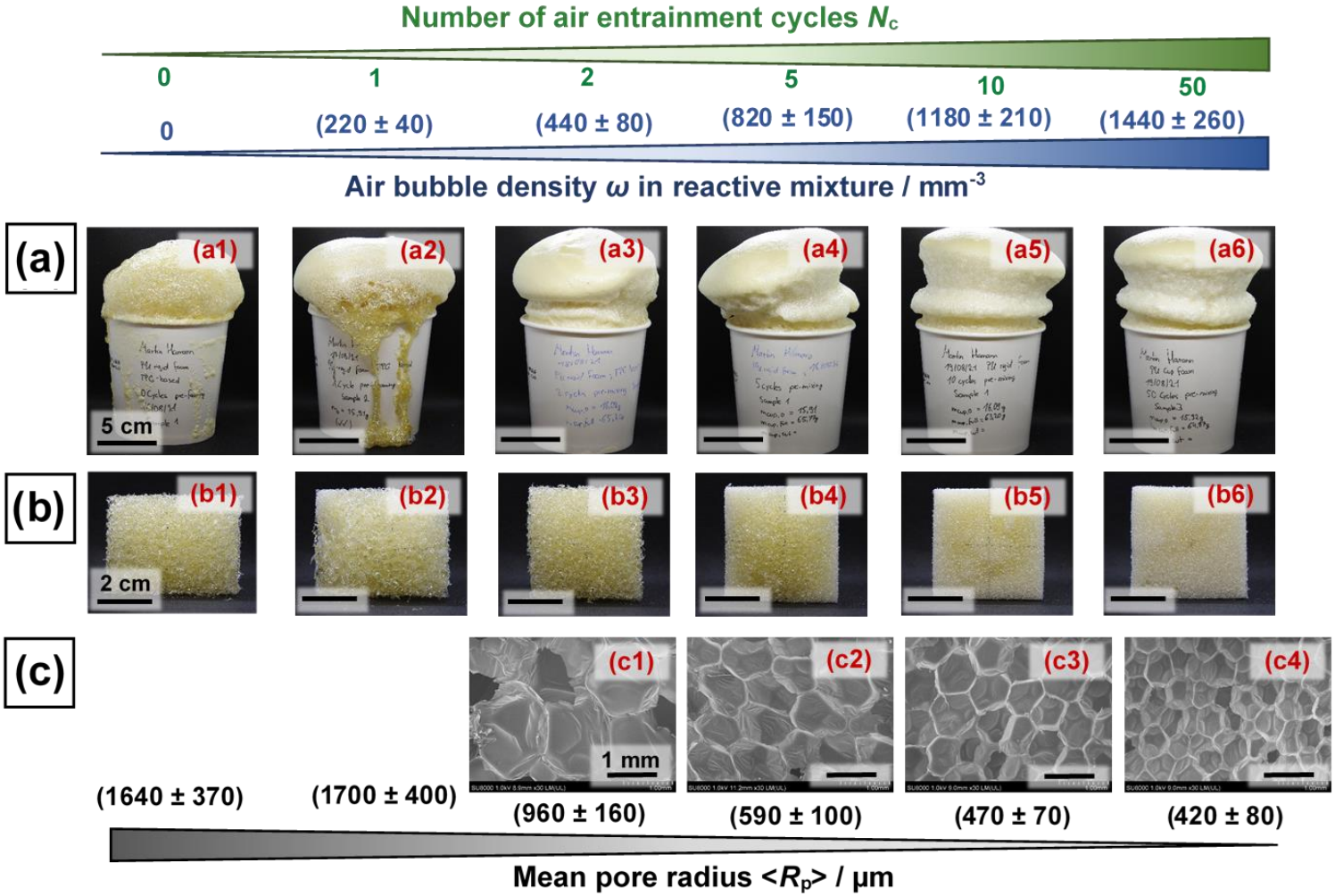

Figure 3: Overview of PUR foams obtained using the double-syringe process with increasing number of air entrainment cycles. (a) Images of the entire cup foams. (b) Images of cubic foam samples cut out of the center of the cup foams. (c) Scanning electron microscopy (SEM) images of slices cut out of the cubic foam samples. Note that for the foams corresponding to N_c = 0 and 1, the SEM images are missing, since the pores were too large. For the case of N_c = 0 and 1, the photographs shown in (b1) and (b2) were used to determine the mean pore size.

Figure 3 demonstrates that with increasing number of air entrainment cycles N_c, i.e. with increasing air bubble density ω_{pre} in the premix and, as a consequence, in the liquid reactive mixture, the mean pore radius $\langle R_p \rangle$ of the corresponding PUR foam decreases. This is supported by Figure 4a, which plots the mean pore radius $\langle R_p \rangle$ as a function of air bubble density ω in the liquid reactive mixture.

Correlation between entrained air bubble density and PUR foam pore size

For small ω, the mean pore radius remains close to 1600 µm (colored zone in Figure 4a), whereas it decreases rapidly beyond an air bubble density of $\omega \approx 250$ - 300 mm^{-3} (blank zone in Figure 4a). This behavior is in good agreement with recent findings of Brondi et al.[6] which can be summarized as follows: without dispersed air bubbles in the premix, nucleation and growth in reactive PUR foam systems can be described by type I classical homogeneous nucleation, where gas bubbles nucleate only due to high levels of gas supersaturation in the liquid phase.[24] Thus, the size of the nucleated bubbles and their growth are determined by physico-chemical properties of the system such as reaction heat and gas supersaturation. In contrast, in the presence of pre-dispersed air bubbles, the released blowing agent vapor has no energy barrier to be overcome in order to nucleate a gas bubble and can therefore readily diffuse into the pre-existing air bubbles (type IV non-classical nucleation).[24] In analogy, we argue that mostly classical homogeneous nucleation due to gas supersaturation (type I) is observed for very low ω (colored zone in Figure 4a). Increasing the air bubble density ω, type I classical nucleation and type IV non-classical nucleation are likely to happen in parallel. However, surpassing this "transition regime", type IV non-classical nucleation becomes the dominating mechanism (blank zone in Figure 4a). In this regime, where the pre-dispersed air bubbles dominate pore formation, a direct link between the air bubble density ω in the liquid reactive mixture and the final PUR foam size is conceivable. Assuming that all the bubbles entrained into the liquid reactive mixture are preserved during PUR foam blowing and take up the liberated blowing agent volume quantitatively to form the pores of the PUR foam, a minimum possible pore size should therefore be accessible. Thus, to estimate a lower bound for the final pore size, we propose a model based on the following approximations:

1. All the released blowing agent volume (cyclopentane vapor + CO_2) is taken up quantitatively by the pre-dispersed air bubbles.
2. The total volume of the pre-dispersed air bubbles is negligible with respect to the total liberated blowing agent volume, i.e. the mean volume $\langle V_b \rangle$ of entrained bubbles is negligible with respect to final, mean pore volume $\langle V_p \rangle$ of the foam ($\langle V_b \rangle \ll \langle V_p \rangle$).
3. The number of air bubbles is preserved as soon as PU foam blowing and PU network formation begin (N_b = const).
4. The density of the initially liquid reactive mixture is approximately the same as the density of the polyurethane polymer that forms the solid continuousphase of the foam. Hence, we neglect the expansion or shrinkage of the fcontinuous phase of the foam during polymerization ($V_{lrm} \approx V_{pol}$). We estimate that this introduces an error of maximally 10%, which is of the order of other experimental errors.

We can then establish the relationship

$$\frac{1}{\langle R_p^3 \rangle} = c \cdot \omega, \qquad \textbf{[2]}$$

with c being

$$c = \frac{4}{3}\pi \cdot \frac{1-\varphi}{\varphi}. \qquad \textbf{[3]}$$

where $\langle R_p^3 \rangle$ is a measure of the mean pore volume and φ is the porosity of the PUR foam. Note that a detailed derivation of Equations [2] and [3] is provided in the supporting information (SI Section 5). This simple model predicts an inverse relation between the final pore *volume* $\langle R_p^3 \rangle$ and the initial air bubble density ω in the liquid reactive premix.

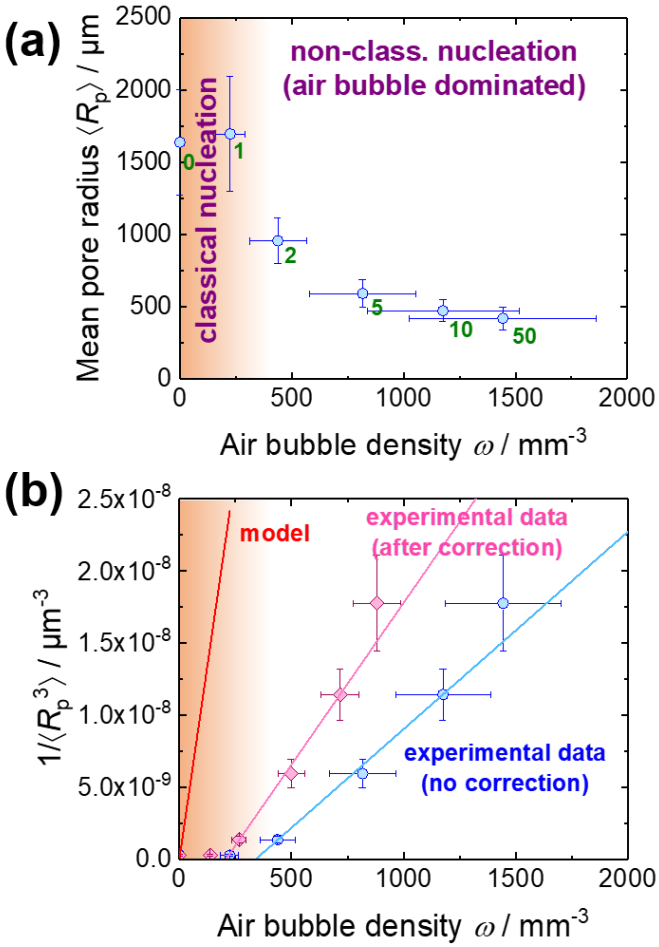

Figure 4: (a) Mean pore radius $\langle R_p \rangle$ of the obtained solid PUR foams versus initial air bubble density ω in the liquid reactive mixture. The green labels represent the number of cycles that was used for the air entrainment step respectively. The colored area represents the regime of homogeneous bubble nucleation, whereas the clear area stands for the non-classical nuclearion regime dominated by the pre-dispersed air bubbles. (b) Mean inverse pore volume $1/\langle R_p^3 \rangle$ of solid PUR foams versus the initial air bubble density ω in the corresponding reactive mixture. The blue points correspond to the raw data, whereas the pink diamonds take into account a correction for bubble ageing during the blending step. The red line represents the proposed model given in Eq. [2].

To check the validity of the model introduced in Eq. [2], we replotted Figure 4a using $1/\langle R_p^3 \rangle$. The resulting diagram is shown in Figure 4b. The red line represents Eq. [2], while the blue data points correspond to the raw experimental data. While both show the same trend predicted by Eq. [2], i.e. $1/\langle R_p^3 \rangle \sim \omega$, they also show a strong discrepancy in the pre-factor. However, this first comparison overlooks a crucial issue: rapid bubble aging through bubble dissolution and Ostwald ripening is affecting the bubble density ω as soon as the air entrainment step is stopped until foam blowing is triggered. Coalescence between air bubbles in the premix is considered negligible at this stage due to the small probability of bubble/bubble encounters thanks to their

low density. Using microscopy of the bubbly premix, we established quantitative estimations of the bubble ageing, which are presented in more detail in the Supplementary Information (SI, Figure S4 and S5). We found that roughly 39% of the air bubbles present in the premix directly after the air entrainment step (see Figure 2) vanish within first 100 seconds due bubble dissolution and gas exchange, 100 s being approximately the delay between the air entrainment step and the beginning of PU foam blowing. We therefore apply this correction for bubble ageing to all the experimental raw data, leading to the pink diamonds shown in Figure 4b.

As can be seen, the slope of the line fitted through the ageing-corrected data in the bubble-dominated regime is closer to the slope of the red line representing the model proposed in Eq. [2]. However, the difference in slope remains a factor of 5: while the slope of Eq. [2] is predicted as 11×10^{-11} $\mu m^{-3}/mm^{-3}$, we find 2.2×10^{-11} $\mu m^{-3}/mm^{-3}$ for the experiment. An explanation for this result could be that we underestimated the extent of bubble ageing prior to the onset of PU foam blowing. This may be due to the fact that the bubble ageing was studied in the premix, i.e. in the A-component only, while the full bubbly reactive mixture also contains 62 vol% of B-component into which air can dissolve. Unfortunately, studying this bubbly reactive mixture via transmitted light microscopy is complicated due to fast reaction kinetics. Moreover, our bubble ageing studies were conducted under static conditions in a quasi-two-dimensional setup (SI Section 3.1) which is very different from the situation present in the double-syringe device. Measuring the air bubble density *in-situ* during double-syringe processing remains a challenge that we have yet to address.

Other than that, our proposed model is based on simple, idealized approximations that may not fully match with the experimental reality. For instance, we calculated that the volume of the reactive system should expand by a factor of ~ 40 upon PUR foam blowing given that the blowing agent vapor and CO_2 are quantitatively integrated into the PUR foam. However, experimentally we find expansion factors between 35 – 37 in our obtained foams (SI Table S2). Last but not least, our model does not take into account potential coarsening of the bubbles while the reactive system expands due to foam blowing. In the same context, coalescence of inflating air bubbles being pushed against each other during foam blowing cannot be ruled out. The monitoring and quantification of both coarsening and coalescence *in-situ* in reacting systems is a delicate challenge that needs further investigation.

Another interesting observation~~s~~ is that the experimentally found line shows an offset on the bubble density-axis unlike the model proposed in Eq. [2]. We hypothesize that this is due to the physical dissolution of a fixed amount of air bubbles in the isocyanate during the blending step

of the premix and the B-component since air is highly soluble in isocyanate. Again, quantifying the actual extent of air bubble dissolution in the B-component during blending remains a challenge due to the hazardous nature of the isocyanate and the fast reaction kinetics. Moreover, a certain proportion of the liberated blowing agent vapor volume might be unavailable for air bubble inflation since a certain solubility of cyclopentane vapor and CO_2 in both the A- and the B-component cannot be denied[30,31].

Due to these different deviations between the experimental reality and the idealized assumptions made in our model, Eq. [2] should therefore be taken as a lower limit for the estimation of the final pore size. However, we emphasize that our data shows that the air bubble density ω in the liquid reactive mixture can in fact be used to alter the mean pore radius $\langle R_p \rangle$ of PUR foams and that, as in the model, there is an inverse relation between the mean pore volume $1/\langle R_p^3 \rangle$ and the air bubble density ω in the air bubble-dominated nucleation regime.

Conclusion

In summary, we describe for the first time the use of a double-syringe mixing device for the preparation of PUR foams. The main advantage of this processing approach is that the entrainment of micrometric air bubbles and the mixing of the reactive components can be systematically decoupled. Moreover, the double-syringe processing technique allows for a controlled variation of the air bubble density in the liquid reactive mixture prior to the onset of foam blowing and PU network formation. We profit from these advantages to analyze the relationship between the air bubble density in the initially liquid reactive mixture and the pore size of the final PUR foam. Our results confirm that the bubble nucleation and growth mechanisms fundamentally depend on the amount of pre-existing air bubbles in the reacting PUR foam system. In absence of dispersed air bubbles (and for very low air bubble densities) in the liquid reactive mixture, bubble nucleation and growth are dominated by supersaturation of the liquid phase with released blowing agent vapor (type I classical homogeneous nucleation). In this case very coarse PUR foams are obtained and the pore size is independent of the initial air bubble density. For high air bubble densities in the liquid reactive mixture, bubble growth is dominated by the inflation of pre-existing air bubbles which serve as reservoirs for released blowing agent vapor which can diffuse into the reservoirs without surpassing any energy barrier (type IV non-classical nucleation). We demonstrated that in the air bubble-dominated regime, there is indeed a distinct correlation between the air bubble density in the

liquid reactive mixture and the mean pore radius of the final PUR foam. For instance, we could reduce the mean pore radius of the foam from 1600 µm to 400 µm only by increasing the amount of pre-dispersed air bubbles within the system. Moreover, we proposed a simple model which predicts the experimentally observed inverse proportionality between the mean pore volume and the air bubble density in the liquid reactive mixture. However, to reach full quantitative agreement between the model and the experiment, all contributions that lead to air bubble and foam ageing need to be addressed quantitatively in future studies. To conclude, we demonstrate how the pore size of PUR foams can be controlled simply via air bubble inclusion into the system prior to foam blowing and PU network formation. These insights highlight the crucial impact of pre-dispersed air bubbles on PUR foam morphology and suggest a new path for foam optimization that focusses primarily on maximizing air bubble entrainment – rather than on the formulation – to reduce the final pore size for optimized thermal insulation. We are confident that the presented approach may not only provide a valuable model experiment to scan formulations in R&D laboratories, but it may also provide concrete suggestions as to how to improve current industrial processes to reach smaller pore sizes at identical formulation for better thermal insulation.

Acknowledgement

The authors gratefully acknowledge Marc Bottinot, Vincent Klein, Jérémy Sanchez, and Rémy Brauge at the Laboratoire de Physique des Solides of the University Paris-Saclay for building the double-syringe device used in this study. The authors would also like to thank Marie-Pierre Krafft for discussions concerning the interaction of fluorocarbons with interfaces, and Manon Jouanlanne, Aurélie Hourlier-Fargette, and Leandro for fruitful exchanges concerning PU formulations and experimental details. Last but not least, the authors gratefully acknowledge the PLAMICS facility of the Institute Charles Sadron for providing access to the SEM.

Conflict of interest

The authors declare that there is no conflict of interest.

Funding

This work has been financed by an ERC Consolidator Grant (agreement 819511 – METAFOAM) and profited also from an IdEx Unistra "Attractivity grant" (Chaire W. Drenckhan). It was conducted in the framework of the Interdisciplinary Institute HiFunMat, as part of the ITI 2021-2028 program of the University of Strasbourg, CNRS and Inserm, was

supported by IdEx Unistra (ANR-10-IDEX-0002) and SFRI (STRATUS project, ANR-20-SFRI-0012) under the framework of the French Investments for the Future Program. Moreover, the authors gratefully acknowledge the financial support granted by BASF SE for this study.

ORCID ID

Martin Hamann https://orcid.org/0000-0001-8573-6217

Supporting information

Detailed supporting information for this article is available online.

References

1. Nejat P, Jomehzadeh F, Taheri MM, et al. A global review of energy consumption, CO2 emissions and policy in the residential sector (with an overview of the top ten CO2 emitting countries). *Renew Sustain Energy Rev* 2015; 43: 843–862.

2. González-Torres M, Pérez-Lombard L, Coronel JF, et al. A review on buildings energy information: Trends, end-uses, fuels and drivers. *Energy Reports* 2022; 8: 626–637.

3. Eling B, Tomović Ž, Schädler V. Current and Future Trends in Polyurethanes: An Industrial Perspective. *Macromol Chem Phys* 2020; 221: 1–11.

4. Reignier J, Alcouffe P, Méchin F, et al. The morphology of rigid polyurethane foam matrix and its evolution with time during foaming – New insight by cryogenic scanning electron microscopy. *J Colloid Interface Sci* 2019; 552: 153–165.

5. Brondi C, Di Maio E, Bertucelli L, et al. The effect of organofluorine additives on the morphology, thermal conductivity and mechanical properties of rigid polyurethane and polyisocyanurate foams. *J Cell Plast* 2021; 58: 121–137.

6. Brondi C, Di Maio E, Bertucelli L, et al. Competing bubble formation mechanisms in rigid polyurethane foaming. *Polymer (Guildf)* 2021; 228: 123877.

7. Merillas B, Villafañe F, Rodríguez-Pérez MÁ. Nanoparticles addition in pu foams: The dramatic effect of trapped-air on nucleation. *Polymers (Basel)* 2021; 13: 1–11.

8. Liu Y, Chen X, Pan J, et al. Effect of microcrystalline cellulose on the preparation and performance of rigid polyurethane foam. *J Cell Plast*. Epub ahead of print 1 September 2022. DOI: 10.1177/0021955X221089434.

9. Omrani I. High performance biobased pour-in-place rigid polyurethane foams from facile prepared castor oil-based polyol: Good compatibility with pentane series blowing agent. *J Cell Plast* 2022; 58: 449–466.

10. Zarzyka I, Pacześniak T, Frącz W. Rigid polyurethane foams modified with borate and oxamide groups – Preparation and properties. *J Cell Plast* 2021; 57: 471–491.

11. Brondi C, Santiago-Calvo M, Di Maio E, et al. Role of Air Bubble Inclusion on Polyurethane Reaction Kinetics. *Materials (Basel)* 2022; 15: 1–18.

12. Ball GW, Hurd R, Walker MG. Conductivity Rigid Urethane Foams. *J Cell Plast* 1970; 6: 66–75.

13. Engels HW, Pirkl HG, Albers R, et al. Polyurethanes: Versatile materials and sustainable problem solvers for today's challenges. *Angew Chemie - Int Ed* 2013; 52: 9422–9441.

14. Ashby MF. Mechanical Properties of Cellular Solids. *Metall Trans A, Phys Metall Mater Sci* 1983; 14 A: 1755–1769.

15. Schuetz MA, Glicksman LR. A basic study of heat transfer through foam insulation. *J Cell Plast* 1984; 20: 114–121.

16. Mills N. *Polymer Foams Handbook*. 1st. Ed. Oxford: Elsevier, 2007.

17. Gibson LJ, Ashby MF. *Cellular solids*. Cambridge: Cambridge University Press, 1997. Epub ahead of print 1997. DOI: https://doi.org/10.1017/CBO9781139878326.

18. Glicksman L, Schuetz M, Sinofsky M. Radiation heat transfer in foam insulation. *Int J Heat Mass Transf* 1987; 30: 187–197.

19. Ashida K. *Polyurethane and Related Foams*. Boca Raton: CRC Press, 2007.

20. Szycher M. *Szycher's Handbook of Polyurethanes*. 2nd Ed. Boca Raton: CRC Press, 2013.

21. Tieke B. *Makromolekulare Chemie: Eine Einführung*. 3rd ed. Weinheim: Wiley VCH, 2014.

22. Kanner B, Decker TG. Urethane Foam Formation— Role of the Silicone Surfactant. *J Cell Plast* 1969; 5: 32–39.

23. Baumhäkel R. Influence of Stirring Velocity and Air Loading on the Formation of

Flexible Urethane Foams. *J Cell Plast* 1972; 8: 304–310.

24. Jones SF, Evans GM, Galvin KP. Bubble nucleation from gas cavities — a review. *Adv Colloid Interface Sci* 1999; 80: 27–50.

25. Zowada R, Foudazi R. Polyfoam: Foam-Templated Microcellular Polymers. *Langmuir* 2020; 36: 7868–7878.

26. Gaillard T, Roché M, Honorez C, et al. Controlled foam generation using cyclic diphasic flows through a constriction. *Int J Multiph Flow* 2017; 96: 173–187.

27. Nastasa V, Samaras K, Pascu ML, et al. Moderately stable emulsions produced by a double syringe method. *Colloids Surfaces A Physicochem Eng Asp* 2014; 460: 321–326.

28. Soullem I, Muller R, Holl Y, et al. A Novel Low-Pressure Device for Production of Nanoemulsions. *Chem Eng Technol* 2012; 35: 1–8.

29. Yu W, Serra CA, Khan IU, et al. Development of an Elongational-Flow Microprocess for the Production of Size- Controlled Nanoemulsions : Batch Operation. *Macromol React Eng* 2016; 11: 1–11.

30. Di Caprio MR, Dal Poggetto G, Pastore Carbone MG, et al. Polyether polyol/CO2 solutions: Solubility, mutual diffusivity, specific volume and interfacial tension by coupled gravimetry-Axisymmetric Drop Shape Analysis. *Fluid Phase Equilib* 2016; 425: 342–350.

31. Di Caprio MR, Immirzi B, Di Maio E, et al. Mass transport and physical properties of polymeric methylene diphenyl diisocyanate/CO2 solutions. *Fluid Phase Equilib* 2018; 456: 116–123.